Journal of Fluorine Chemistry 211 (2018) 109–118

Contents lists available at ScienceDirect

Journal of Fluorine Chemistry

journal homepage: www.elsevier.com/locate/fluor

Rate constants and C—C bond scission ratios for hydrolysis of 2,2,3-trifluoro-3-(trifluoromethyl)oxirane determined by means of a closed-circulation reactor

Shuzo Kutsuna

National Institute of Advanced Industrial Science and Technology (AIST), 16-1 Onogawa, Tsukuba, 305-8569, Japan

ARTICLE INFO

Keywords:
Fluorinated epoxide
Physicochemical property
pH-independent hydrolysis
Hydroxide-catalyzed hydrolysis
Two-film model
Atmospheric lifetime

ABSTRACT

The hydrolysis rate constant of 2,2,2-trifluoro-3-(trifluoromethyl)oxirane (hexafluoropropene oxide; HFPO), a versatile precursor of fluorinated chemicals, was determined at 279–307 K, and the rate of hydrolysis was used to estimate the tropospheric lifetime of HFPO with respect to hydrolysis in clouds or uptake by the ocean. The low solubility of HFPO in water made it difficult to determine the hydrolysis rate constant because of mass-transfer limitation between the gas and liquid. A closed-circulation reactor was used to measure the rate of decrease of the partial pressure of HFPO while an HFPO-air mixture flowed over a stirred test solution under various experimental conditions. The rate of hydrolysis increased as the OH^- concentration increased in an aqueous NaOH solution but was almost independent of the H_2SO_4 concentration in aqueous H_2SO_4 solutions. Much scissioning of C—C bonds in HFPO produced carbon monoxide and trifluoroacetate in aqueous NaOH, but similar scissioning did not in water or aqueous H_2SO_4. The first-order rate constant for the pH-independent hydrolysis (k_{water} in s^{-1}), the bimolecular rate constant for the hydroxide-catalyzed hydrolysis, and the temperature dependence of these parameters were estimated by simultaneously fitting equations based on a two-film model to the time series of HFPO partial pressures under different experimental conditions. The equations included the rate constants as common parameters. The product of k_{water} and the Henry's law constant, K_H (M Pa^{-1}), at a temperature of T (K) was determined to be $k_{water} \times K_H = 3.7 \times 10^{-11} \exp[-3300 \times (T^{-1} - 1/298.2)]$. The tropospheric lifetime of HFPO estimated using this equation indicates that removal of HFPO via hydrolysis in clouds is probably not a substantial sink of HFPO and suggests that, in the absence of other atmospheric sinks of HFPO, hydrolysis of HFPO in the ocean would be the major sink of HFPO.

1. Introduction

2,2,2-Trifluoro-3-(trifluoromethyl)oxirane (hexafluoropropene oxide; HFPO; $CF_3CF(-O-)CF_2$) is a versatile precursor of fluorinated chemicals [1]. Its epoxide functional group has special features that allow it to play important roles in fluorinated chemical synthesis; HFPO has therefore been widely used in fluorochemical industrial processes. Much information about this use has accumulated, but little is known about the fate of HFPO after it is released into the environment. There is an absence of information about the physicochemical properties of HFPO, such as the rate constants for its gaseous reactions with OH radicals, which are relevant to processes involved in its removal from the atmosphere.

A potential mechanism for removing HFPO from the atmosphere is hydrolysis in cloud droplets or uptake by the ocean, because HFPO is known to hydrolyze in water at ambient temperature via Eq. (1) [2] :

$$CF_3CF(-O-)CF_2 + 3H_2O \rightarrow CF_3C(OH)_2COOH + 3F^- + 3H^+ \quad (1)$$

The rate constant for this hydrolysis, k_{hyd}, must be known to estimate the atmospheric lifetime of HFPO with respect to hydrolysis in clouds or uptake by the ocean, but, to the author's knowledge, no values of k_{hyd} are available in peer-reviewed journals. The objective of this study was to determine k_{hyd} at ambient temperatures.

Hydrolysis of epoxides such as oxirane ($CH_2(-O-)CH_2$) is a long-standing issue in the context of industrial applications and biological activities, and has been experimentally and theoretically investigated [3–12]. Furthermore, atmospheric hydrolysis of second-generation epoxides derived from isoprene has recently been studied with respect to environmental issues because these reactions can contribute to formation of secondary organic aerosols [13]. Experimental results suggest a rate expression that includes three kinetically distinguishable paths for the hydrolysis as follows [3,6]:

$$k_{hyd} = k_{water} + k_a [H_3O^+] + k_b [OH^-], \quad (2)$$

where k_{water} is the first-order rate constant for the pH-independent

E-mail address: s-kutsuna@aist.go.jp.

https://doi.org/10.1016/j.jfluchem.2018.04.013
Received 17 March 2018; Received in revised form 18 April 2018; Accepted 19 April 2018
Available online 22 April 2018
0022-1139/

hydrolysis; k_a is the bimolecular rate constant for the acid-catalyzed hydrolysis; and k_b is the bimolecular rate constant for the hydroxide-catalyzed hydrolysis. For oxirane, values at 298 K have been reported to be $k_{water} = 5.7 \times 10^{-7}$ s^{-1}; $k_a = 9 \times 10^{-3}$ M^{-1} s^{-1}; and $k_b = 1 \times 10^{-4}$ M^{-1} s^{-1} [8]. The hydrolysis begins with the cleavage of a C—O bond of the epoxide ring. In the case of hydroxide-catalyzed and pH-independent paths, hydrolysis begins with a bimolecular nucleophilic substitution that involves the breaking of the epoxide C—O bond and formation of a covalent bond between the nucleophile and epoxide. The dominant hydrolytic products are diols such as glycols without C—C bond scissions for most epoxides.

For halogenated epoxides, hydrolysis of chlorinated ethene oxides such as trichloroethylene oxide [10,11] and tetrachloroethylene oxide [12] has been studied with particular emphasis on biological issues. The values of k_{water} and k_a for trichloroethylene oxide are more than 10^5 and 3 times, respectively, those for oxirane. The fact that carbon monoxide is the main hydrolytic product from trichloroethylene oxide and tetrachloroethylene oxide indicates that a C—C bond scission occurs after C—O bond cleavage of the epoxide ring during hydrolysis of these halogenated epoxides.

The relatively low solubility in water and absence of near-ultraviolet and visible absorption of HFPO may make it difficult to determine the value of k_{hyd} for HFPO. In this study, a reactor with a closed circulation system was used to observe decreases of the partial pressure of HFPO at various stirring speeds in test solutions with different pH values (e.g. deionized water and aqueous NaOH). The dependence of the rate of decrease of the partial pressure of HFPO on the stirring speed of the test solutions suggested that the rates of gaseous HFPO hydrolysis were limited by mass-transfer between the gas and liquid. A two-film model [14] was therefore used to determine values of k_{hyd} by fitting simultaneous equations, with k_{water} and k_b as common parameters, to the time series of HFPO partial pressures observed under different experimental conditions. Degradation products were found to differ between reactions in water and aqueous NaOH, and much C—C bond scissioning occurred in aqueous NaOH.

2. Results

2.1. Decreases of HFPO during the experimental runs at various stirring speeds of the test solutions with different pH values

Fig. 1 shows the residence ratio, P_t/P_0, of HFPO on a logarithmic scale as a function of time for each experimental run in which an HFPO-air mixture flowed over deionized water at 295.9 K in the closed-circulation reactor. The parameter P_t is the partial pressure of HFPO at time t, and P_0 is the initial partial pressure of HFPO. In each experimental run, the deionized water was stirred at a prescribed rate that ranged from 0 to 1200 rpm. At 60 min, the circulation route was changed so that the gas mixture flowed over the deionized water. The resulting increase in the total volume corresponded to a 29% decrease in the partial pressure of HFPO and a corresponding abrupt decrease of the residence ratio at 60 min (Fig. 1).

When the HFPO-air mixture flowed over deionized water, the partial pressure of gaseous HFPO decreased with time. This observation, combined with the detection of degradation products such as F^- (described later), clearly indicated that hydrolysis of HFPO proceeded in the deionized water. The partial pressure of HFPO decreased with time according to first-order kinetics:

$$\ln(P_t/P_0) = -k_1 t, \quad (3)$$

where k_1 is the first-order rate constant for the rate of change of the partial pressure of gaseous HFPO.

That values of k_1 increased with increasing stirring speeds of the deionized water suggested that the rate of change of gaseous HFPO was limited by mass transfer of HFPO between the gas and liquid. The data

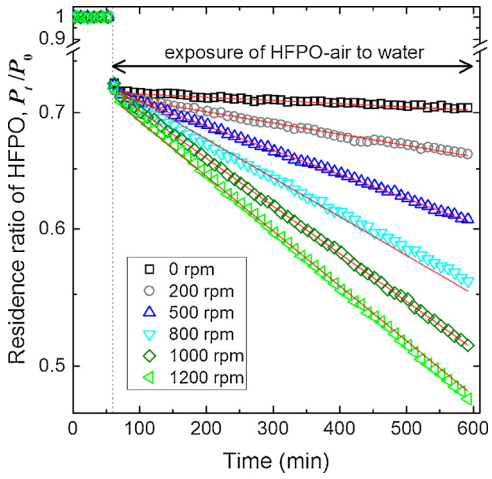

Fig. 1. Time course of the residence ratio of gas-phase HFPO (P_t/P_0) when the HFPO-air mixture was allowed to flow over deionized water stirred at rates ranging from 0 to 1200 rpm at a temperature of 295.9 K. The values of P_0 were 20.6, 20.8, 19.9, 20.6, 20.0, and 20.3 Pa for each experimental run in order of increasing stirring rates from 0 to 1200 rpm. Red lines indicate the values calculated from the fitting procedure (Section 2.2) (For interpretation of the references to colour in this figure legend, the reader is referred to the web version of this article).

in Fig. 1 alone could not be used to determine the value of k_{hyd}. A relationship such as Eq. (2) imposed further constraints on the value of k_{hyd}, as discussed later (Section 3.2). Therefore, similar experiments were performed for 10–50 mM aqueous NaOH solutions stirred at 800, 1000, and 1200 rpm at 295.9 K (Fig. 2, panels a, b, and d) and for 10–30 mM aqueous H_2SO_4 solutions stirred at 1000 rpm at 295.9 K (Fig. 2, panel c).

The partial pressure of HFPO decreased with time according to first-order kinetics (Eq. (3)) in each experimental run (Fig. 2). Fig. 3 plots the k_1 values obtained from the data in Fig. 2 against the nominal molar concentrations of NaOH and H_2SO_4. The k_1 values increased with increasing concentration of NaOH but were almost independent of the concentration of H_2SO_4 in the concentration range examined. Fig. 3 thus suggests that Eq. (4) applies to the hydrolysis of HFPO at NaOH concentrations of 0–50 mM.

$$k_{hyd} = k_{water} + k_b [OH^-] \quad (4)$$

2.2. Evaluation of hydrolysis rate constants of HFPO by fitting to the time series of HFPO partial pressures observed under different reaction conditions

Under the experimental conditions examined, the decrease of gaseous HFPO was apparently limited by mass transfer between the gas and liquid phases (Fig. 1). Using a two-film model to describe the mass transfer process [14] together with Eq. (4) enabled me to simulate the time series of gaseous HFPO as follows:

$$dP_t/dt = -a_1 k_m (K_H P_t - C_t) \quad (5)$$

$$dC_t/dt = a_2 k_m (K_H P_t - C_t) - (k_{water} + k_b [OH^-]) C_t, \quad (6)$$

where k_m, in dm^3 s^{-1}, is the volumetric mass transfer coefficient; K_H, in M Pa^{-1}, is the Henry's law constant of HFPO; and C_t, in M, is the bulk concentration of HFPO in the test solutions. Here the first-order rate constant for the pH-independent hydrolysis of HFPO, k_{water}, is represented in s^{-1}; the bimolecular rate constant for the hydroxide-catalyzed hydrolysis, k_b, is represented in M^{-1} s^{-1}. The constants a_1 and a_2 are defined as follows:

$$a_1 = RT_a / (10^{-3} V_G), \quad (7)$$

$$a_2 = 1/V_L, \quad (8)$$

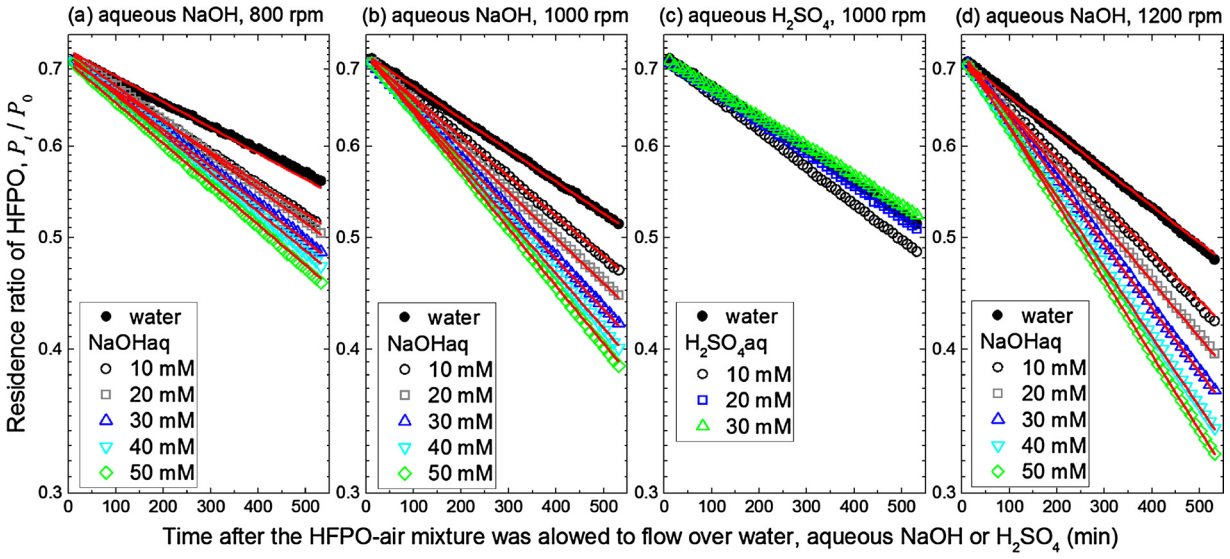

Fig. 2. Time series of the residence ratio of gas-phase HFPO (P_t/P_0) after the HFPO-air mixture was allowed to flow over aqueous NaOH (10–50 mM, stirred at 800, 1000, or 1200 rpm) or aqueous H_2SO_4 (10–30 mM, stirred at 1000 rpm) at a temperature of 295.9 K. Red lines indicate the values calculated from the fitting procedure (section 2.2) (For interpretation of the references to colour in this figure legend, the reader is referred to the web version of this article).

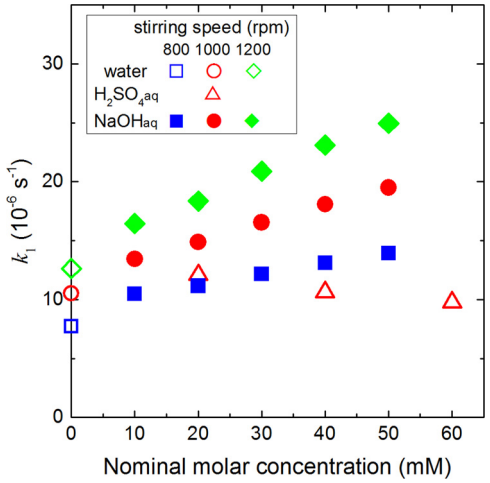

Fig. 3. Dependence of the rate constant k_1, which was deduced from the data shown in Fig. 2, on the concentrations of aqueous NaOH and aqueous H_2SO_4.

where R is the universal gas constant (8.314 J mol^{-1} K^{-1}); T_a is room temperature (298 K); 10^{-3} is a conversion factor (m^3 dm^{-3}); V_G is the gas-phase volume of the closed-circulation reactor (0.962 dm^3); and V_L is the volume of the test solutions (0.180 dm^3). Values of k_m here involved only mass transfer resistance in the liquid phase because of the relatively slow decay rate of gaseous HFPO and its low solubility in water.

The values of k_{water} and k_b were determined by fitting Eqs. (5) and (6) to all the data with k_{water} and k_b as common parameters. In this procedure, the ratio (α) of the partial pressure of HFPO just after the circulation route was changed at 60 min, to P_0 was also fitted as a parameter for each experimental run. The value of α was expected to be 0.71, as explained in Section 2.1. Eqs. (5) and (6) were used to describe all the time series of HFPO partial pressures for deionized water and aqueous NaOH test solutions at 295.9 K.

The fitting was performed using the parameter-fitting routine of the FACSIMILE software (MCPA Software Ltd, UK). This parameter-fitting routine consisted of two phases. During the first phase, a number of simulation runs with different parameter values were carried out to find the combination of parameter values that minimized the sum of squared residuals. The residual, R_{ij}, is defined as

$$R_{ij} = (\nu_{ij} - u_{ij})/\sigma_{ij}, \quad (9)$$

where j corresponds to the jth point in time and i to the ith time series; ν_{ij} is the observed partial pressure of HFPO and u_{ij} is the corresponding calculated value; σ_{ij} is a weighting error. In the fitting procedure, a constant value of σ_{ij} (0.032 Pa) was used for all the data. When satisfactory convergence to a minimum sum of squared residuals had been achieved, the second phase was started. During the second phase, the sensitivity matrix that characterized the dependence of R_{ij} on each parameter at the best parameter values was recomputed. The sensitivity matrix was used to carry out a statistical analysis of the goodness of fit and to estimate the variances and covariances of the fitting parameters. Occasionally some of the final parameter values differed slightly from the values at the end of the first phase.

With K_H assigned the reported value of 9.5×10^{-9} M Pa^{-1} [15], the parameter values were obtained as listed in Table 1. The obtained values of α were 0.71–0.73, very similar to the expected value of 0.71.

Figs. 1 and 2 show the values of P_t/P_0 calculated from the fitting procedure. The values of the parameters in Table 1 reproduce the time series of gaseous HFPO partial pressures under different conditions. The values of k_m increased with stirring speed. The values of k_{water} and k_b were 6000 and 1000 times, respectively, the values at 298 K of oxirane [8]. The value of k_{water} was half the corresponding value for trichloroethylene oxide at 298 K [10].

Table 1
Values at 295.9 K of k_{water}, k_b, and k_m determined by fitting Eqs. (5) and (6) to all the time series of HFPO partial pressures.

k_{water} (s^{-1}) [a]			(3.68 ± 0.04) × 10^{-3}			
k_b (M^{-1} s^{-1}) [a]			(1.61 ± 0.07) × 10^{-1}			
stirring speed (rpm)	0	200	500	800	1000	1200
k_m (10^{-4} dm^3 s^{-1}) [a]	0.3 ± 0.0	1.2 ± 0.0	3.3 ± 0.1	7.5 ± 0.1	12.5 ± 0.3	20.1 ± 0.7

[a] Error bounds are 90% confidence intervals based on the fitting procedure.

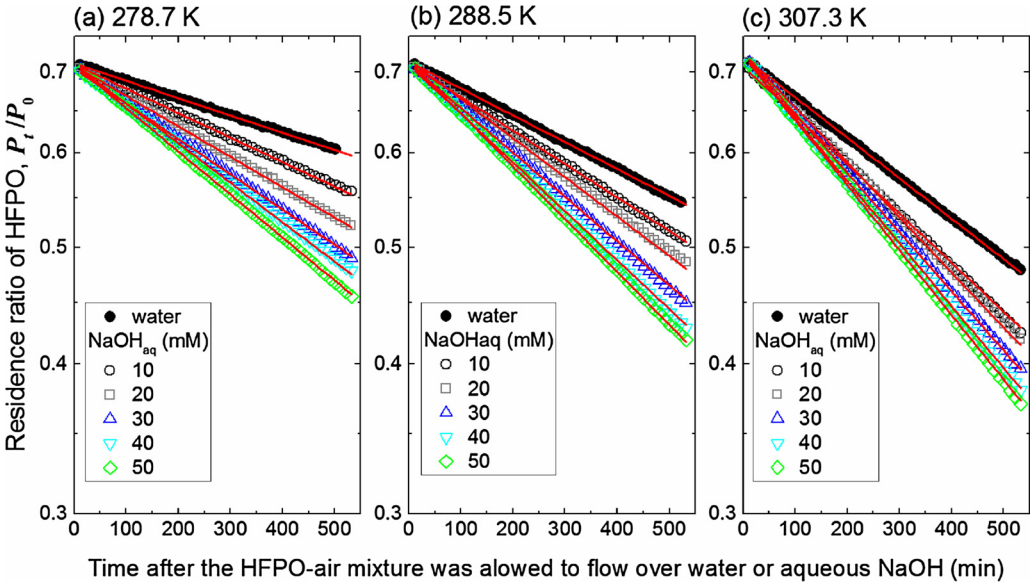

Fig. 4. Time series of the residence ratios of gas-phase HFPO (P_t/P_0) when the HFPO-air mixture was allowed to flow over water or aqueous NaOH test solutions stirred at 1000 rpm at each temperature. Red lines indicate values calculated from the fitting procedure (For interpretation of the references to colour in this figure legend, the reader is referred to the web version of this article).

2.3. Temperature dependence of the rate constants for hydrolysis of HFPO

Experimental runs similar to those shown in Fig. 2 were carried out for deionized water and 10–50 mM aqueous NaOH stirred at 1000 rpm and at temperatures of 278.7 K, 288.5 K, and 307.3 K (Fig. 4). The partial pressure of HFPO decreased with time according to first-order kinetics (Eq. (3)) in each experimental run.

In a way similar to that described in Section 2.2, Eqs. (5) and (6) were fit to all the time series of HFPO partial pressures at each temperature, with k_{water}, k_b, and k_m as common parameters at each temperature. Results of this procedure are shown in Table 2. The value of α was also fitted as a parameter in each experimental run. The values of α obtained by this procedure were almost equal to the expected value of 0.71. In this fitting, the temperature-dependence of K_H (M Pa^{-1}) was assumed to be represented by Eq. (10) [15].

$$K_H(T) = 8.8 \times 10^{-9} \exp[3000 \times (T^{-1} - 1/298.15)] \quad (10)$$

Values of P_t/P_0 calculated with this fitting procedure are shown in Fig. 4. The values of the parameters in Table 2 reproduced the time series of gaseous HFPO partial pressures at each temperature.

Fig. 5 shows the values of k_{water} and k_b determined by this procedure (Tables 1 and 2) on a logarithmic scale against the inverse of temperature. The plot for k_{water} is linear, and the values of k_{water} can be expressed by the Arrhenius equation:

$$k_{water}(T) = k_{water}(T_0) \times \exp[-\Delta E_{water}/R \times (T^{-1} - T_0^{-1})], \quad (11)$$

where T_0 is 298.2 K and ΔE_{water} (kJ mol^{-1}) is the activation energy for the pH-independent hydrolysis of HFPO. From the regression line fit to the data in Fig. 5, the value of k_{water} at 298.2 K was determined to be $(4.2 \pm 0.4) \times 10^{-3}$ s^{-1}, and the value of ΔE_{water} was estimated to be 52 ± 7 kJ mol^{-1}. The error bounds are the 95% confidence intervals based on the regression equation.

The regression equation for the plot of k_b with Eq. (12) likewise gave values of k_b at 298.2 K and ΔE_b: $k_b(T_0) = (1.9 \pm 0.5) \times 10^{-1}$ M^{-1} s^{-1}; $\Delta E_b = 61 \pm 20$ kJ mol^{-1}. The large error bounds for ΔE_b suggest that ΔE_b might vary in the temperature range 278.7–307.3 K.

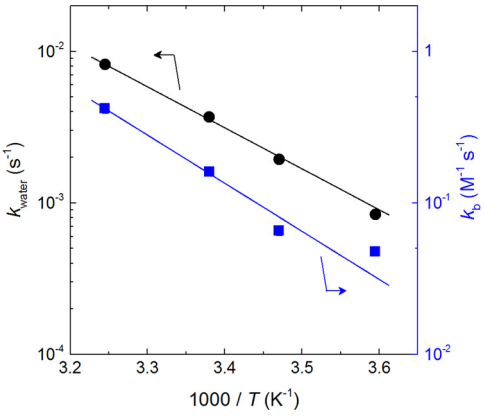

Fig. 5. Temperature-dependence of k_{water} and k_b. The two y axes correspond to data points with the same color. Lines represent regression Eqs. (11) and (12).

$$k_b(T) = k_b(T_0) \times \exp[-\Delta E_b/R \times (T^{-1} - T_0^{-1})] \quad (12)$$

2.4. Degradation products from hydrolysis in deionized water, aqueous H_2SO_4, and aqueous NaOH

In the deionized water test solutions exposed to gas mixtures containing HFPO, F^- was detected as a degradation product via ion chromatography. The chromatogram shows the F^- peak at a retention time of about 9 min and suggests that another species was produced with a retention time of about 21 min (Fig. 6a). The amount of F^- was

Table 2
Values of k_{water}, k_b, and k_m determined for the test solutions stirred at 1000 rpm at each temperature by fitting Eqs. (5) and (6) to all the time series of HFPO partial pressures.

temperature (K)	k_{water} (s^{-1}) [a]	k_b (M^{-1} s^{-1}) [a]	k_m (10^{-4} dm^3 s^{-1}) [a]
278.7	$(0.84 \pm 0.01) \times 10^{-3}$	$(0.48 \pm 0.03) \times 10^{-1}$	6.3 ± 0.3
288.5	$(1.93 \pm 0.03) \times 10^{-3}$	$(0.66 \pm 0.05) \times 10^{-1}$	12.4 ± 0.9
307.3	$(8.17 \pm 0.14) \times 10^{-3}$	$(4.18 \pm 0.28) \times 10^{-1}$	16.0 ± 0.3

[a] Error bounds are 90% confidence intervals based on the fitting procedure.

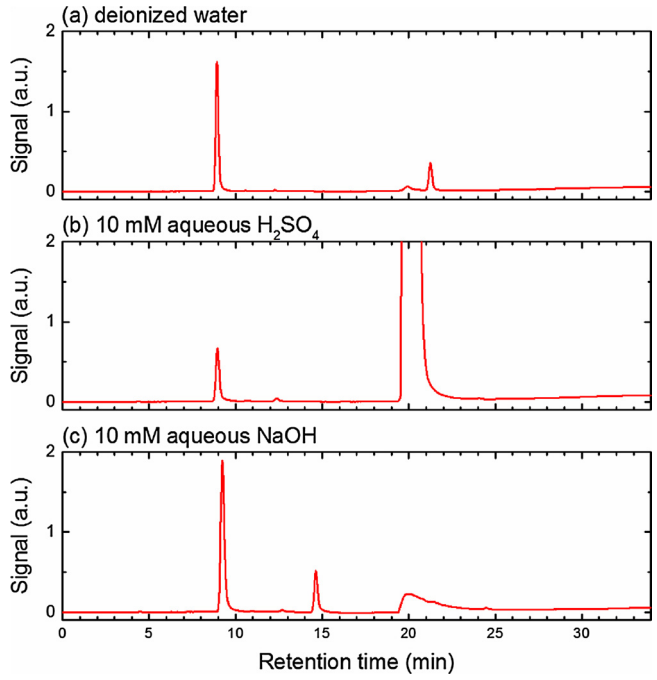

Fig. 6. Ion chromatograms of test solutions exposed to an HFPO-air mixture for about 9 h at 295.9 K with stirring at 1000 rpm: the test solutions were deionized water (panel a), a 10 mM aqueous H_2SO_4 solution (panel b), and a 10 mM aqueous NaOH solution (panel c). The test solution in panel b had been neutralized with an aqueous NaOH solution before ion chromatographic analysis.

2.9 ± 0.1 times the decrease in the amount of HFPO (Fig. 7a). Error bounds are 95% confidence intervals based on the regression line fit that passes through the origin to the corresponding data points, and so are in this section. The signal intensity of the ion chromatogram peak at ~21 min was also proportional to the decrease in the amount of HFPO. No gaseous products such as carbon monoxide were observed (Fig. 8a). These results are consistent with the scenario that HFPO was hydrolyzed in water mainly via Eq. (1). The peak in the ion chromatogram at ~21 min might have been $CF_3C(OH)_2COOH$, which would have dissociated into $CF_3C(O^-)_2COO^-$ in the aqueous KOH solutions used as an eluent in the ion chromatographic analysis.

In the aqueous H_2SO_4 test solutions (Fig. 7b), F^- was detected as a degradation product of HFPO with a yield of 2.6 ± 0.7 per HFPO degraded (in accord with Eq. (1)), similar to the yield of F^- in deionized water. The extent of formation of $CF_3C(OH)_2COOH$ was unclear because the ion chromatogram peak attributable to $CF_3C(OH)_2COOH$ was overlapped by a large SO_4^{2-} peak (Fig. 6b).

In the aqueous NaOH test solutions (Fig. 7b), F^- was detected as a degradation product of HFPO, and the amount of F^- was proportional to the decrease in the amount of HFPO. The yield was almost three (2.7 ± 0.1) F^- per HFPO, similar to the yields observed in deionized water and aqueous H_2SO_4. In contrast, the ion chromatogram peak attributable to $CF_3C(OH)_2COOH$ did not appear in ion chromatograms of aqueous NaOH test solutions (Fig. 6c). Instead, $CF_3C(O)O^-$ was detected as an ion chromatogram peak at a retention time of ~14 min. The concentrations of $CF_3C(O)O^-$ were determined by ion-exclusion chromatography; the yield was about 1 (0.92 ± 0.02) $CF_3C(O)O^-$ per HFPO (Fig. 7b). Furthermore, carbon monoxide was detected as a gaseous product (Fig. 8b). Neither $CF_3C(O)O^-$ nor carbon monoxide was observed in the deionized water and aqueous H_2SO_4 test solutions.

Fig. 9 plots the partial pressure of carbon monoxide (P_{CO} in Pa) versus the decrease of the partial pressure of HFPO ($-\Delta P_{HFPO}$ in Pa) for all the experimental runs in aqueous NaOH test solutions at 295.9 K. The increases of the partial pressures of carbon monoxide were proportional to the decreases of the partial pressures of HFPO; the ratio of the former to the latter (m) for each concentration of NaOH was regressed in accord with Eq. (13).

The values of m were almost constant (ca. 0.87), independent of concentrations of NaOH and stirring speeds of the test solutions.

$$P_{CO} = m \times (-\Delta P_{HFPO}) \quad (13)$$

These results clearly indicate that hydrolysis of HFPO in aqueous NaOH test solutions involved much C—C bond cleavage. Furthermore, the proportionality of the relationship between $-\Delta P_{HFPO}$ and P_{CO} (Fig. 9) suggests that hydrolysis of HFPO was a rate-determining step

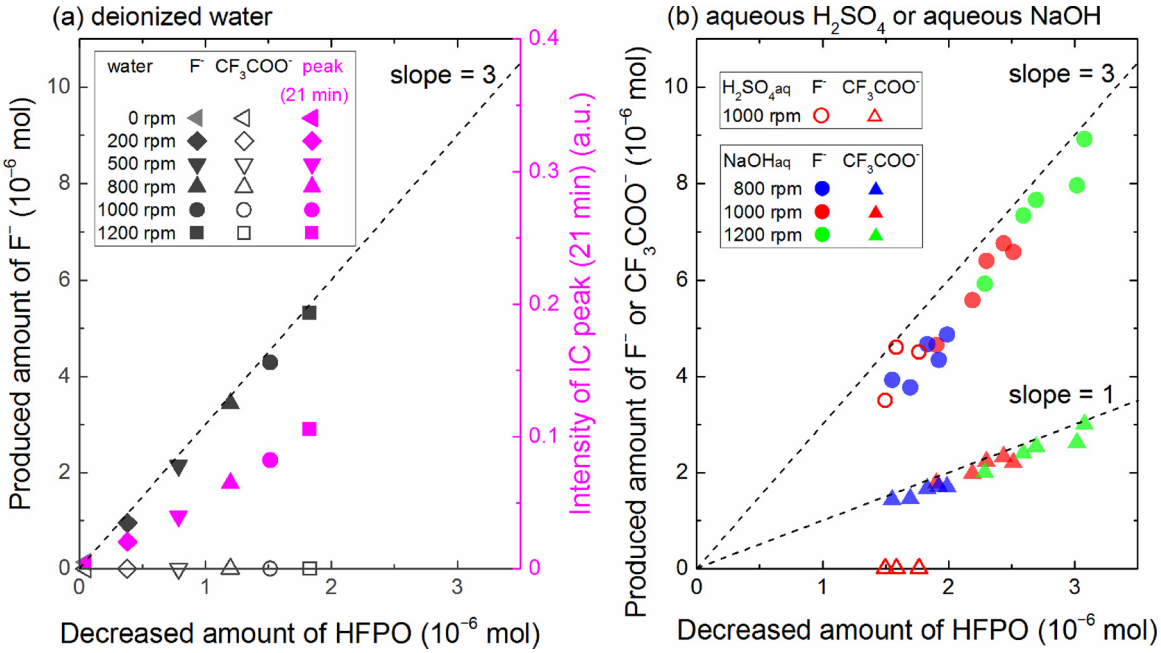

Fig. 7. The amount of degradation products versus the decrease in the amount of HFPO for each experimental run in deionized water stirred at 200–1200 rpm (panel a) and in aqueous H_2SO_4 stirred at 1000 rpm or aqueous NaOH solutions stirred at 800–1200 rpm (panel b). All the experimental runs were performed at 295.9 K. The dashed lines have slopes of 1 or 3, as indicated.

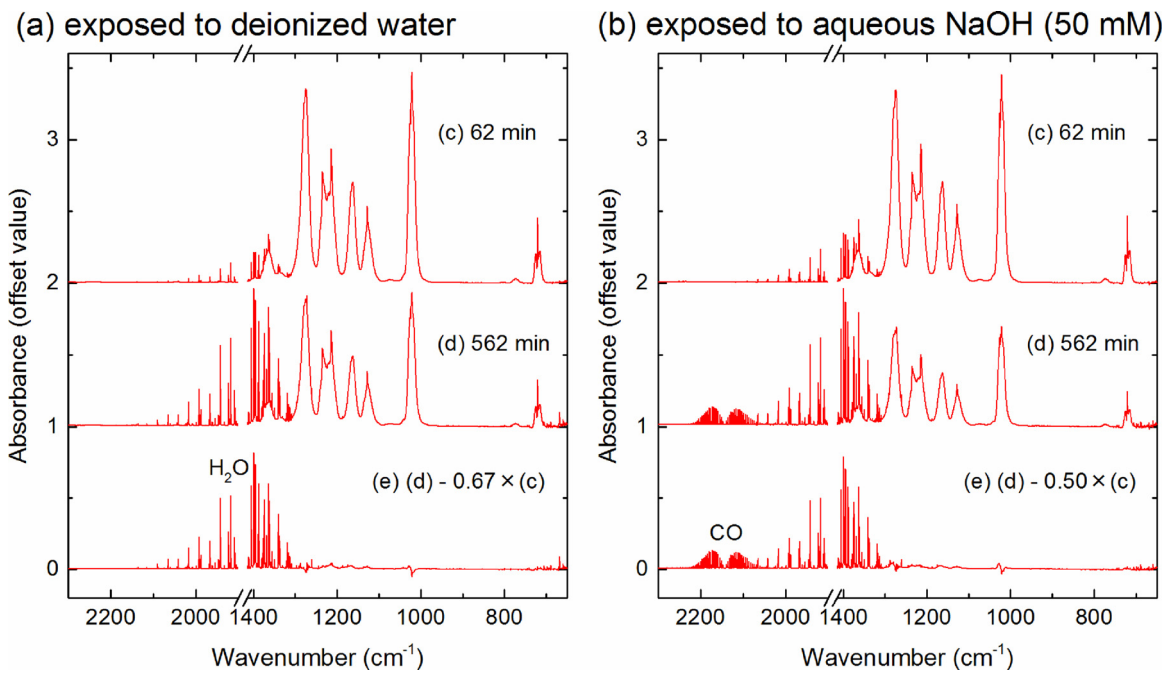

Fig. 8. IR spectra of HFPO-air mixtures exposed to deionized water (panel a) and an aqueous NaOH solution (50 mM, panel b) stirred at 1000 rpm and at 295.9 K. In panels a and b, (e) is the difference between the spectrum in (d) and 0.67 or 0.50 times the spectrum in (c), respectively.

for formation of carbon monoxide. In the aqueous NaOH test solutions, hydrolysis of HFPO proceeded primarily via Eq. (14) instead of Eq. (1):

$$CF_3CF(-O-)CF_2 + OH^- + H_2O \rightarrow CF_3COO^- + CO + 3F^- + 3H^+ \quad (14)$$

A similar experiment was performed for a 4×10^{-2} mM aqueous NaOH test solution stirred at 1000 rpm at 295.9 K to examine how hydrolysis of HFPO (Eqs. (1) or (14)) depended on lower concentration of OH^- (Fig. S1). Scissioning of C–C bonds in HFPO produced carbon monoxide for ca. 4 h after the HFPO-air mixture began to flow over the aqueous NaOH test solution, but it did not in the following duration; scheme for hydrolysis of HFPO was expected to change from Eq. (14) to (1). This change probably arose from the decrease in OH^- concentration with hydrolysis via Eq. (14). Four mole of OH^- was consumed per a mole of HFPO reacted according to Eq. (14). Fig. 10 plots the relationship between $-\Delta P_{HFPO}$ and P_{CO}. Fig. 10 also shows the calculated concentration of OH^- involving the aforementioned decrease in the test solution ($[OH^-]_{calc}$). It indicates that hydrolysis of HFPO proceeded via Eq. (1) in the OH^- concentration range of less than ca. 2×10^{-5} M. Because the OH^- concentration range of less than 2×10^{-5} M corresponds to less than ca. 9 of pH, hydrolysis of HFPO is expected to proceed primarily via Eq. (1) in the environment as discussed in Section 3.3.

3. Discussion

3.1. Potential degradation scheme of HFPO in water and aqueous NaOH

Degradation products resulting from the hydrolysis of HFPO differed distinctly between reactions carried out in deionized water and aqueous NaOH. This difference might seem strange, because the reaction rates for the hydrolysis of HFPO differed by less than a factor of two (Fig. 3) between the deionized water and the aqueous NaOH test solutions. A scheme to reconcile the large difference in the degradation products with the comparatively small change of reaction rates may include dissociation of an intermediate **5** in the aqueous NaOH test solutions (Scheme 1).

In both deionized water and aqueous NaOH, hydrolysis of HFPO **1** (Scheme 1) could be initiated via attack by H_2O or OH^- as a nucleophilic reagent at the CF_3–CF– position (secondary position) [16] followed by formation of an intermediate of $CF_3C(O)C(O)F$ **3** by analogy with the mechanism proposed for hydrolysis of trichloroethylene oxide

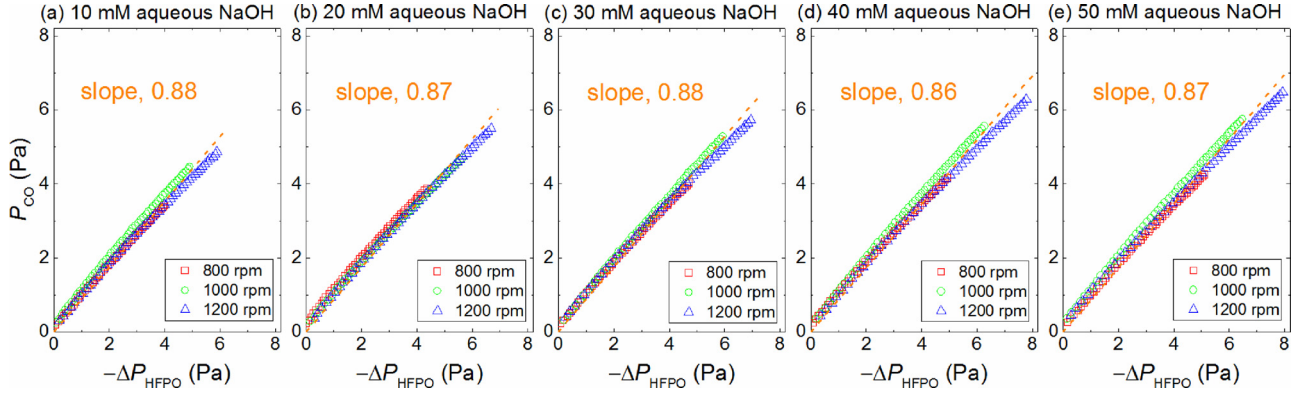

Fig. 9. Increase in partial pressure of carbon monoxide versus decrease of the partial pressure of HFPO for each experimental run in aqueous NaOH stirred at 800, 1000, and 1200 rpm at 295.9 K. Orange dashed lines represent the regression using Eq. (13); orange numbers indicate the slope obtained with the regression.

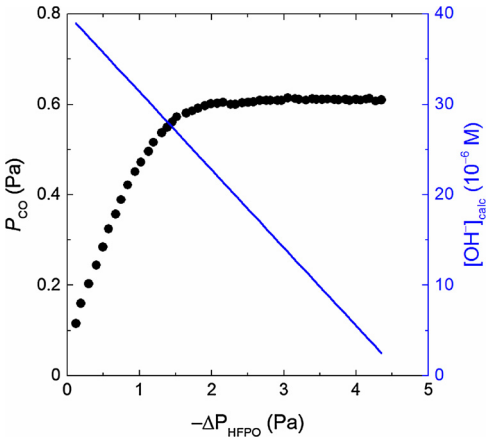

Fig. 10. Increase in partial pressure of carbon monoxide (left axis) and the concentration of OH^- calculated (right blue axis) versus decrease of the partial pressure of HFPO for the experimental run in 4×10^{-2} mM aqueous NaOH stirred at 1000 rpm at 295.9 K. The two y axes correspond to data points or a line with the same color (For interpretation of the references to colour in this figure legend, the reader is referred to the web version of this article).

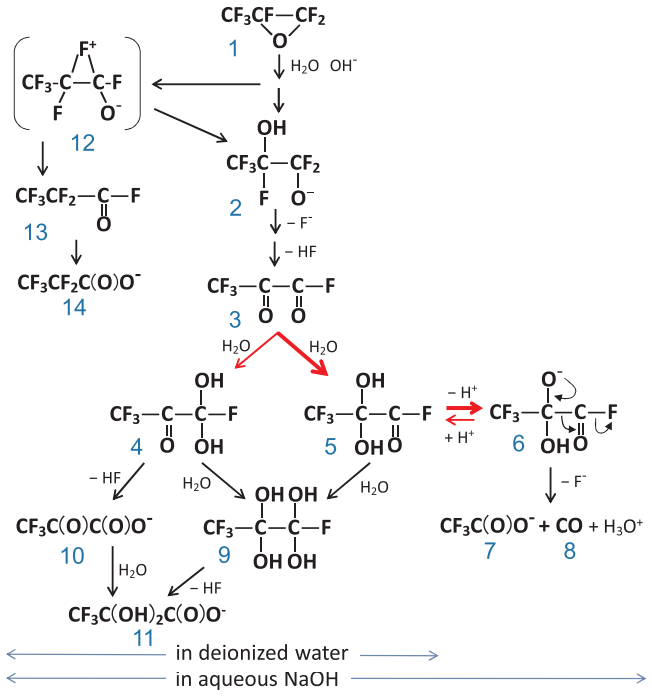

Scheme 1. Possible reaction scheme for hydrolysis of HFPO in deionized water and aqueous NaOH.

[10,11]. This intermediate **3** was hydrated to either $CF_3C(O)C(OH)_2F$ **4** or $CF_3C(OH)_2C(O)F$ **5**. The $-C(OH)_2F$ group in the intermediate **4** could easily be transformed into $-C(O)O^-$. No carbon monoxide **8** was therefore produced from **4**. Carbon monoxide could, however, be produced from the hydrated intermediate **5**.

The degradation scheme of intermediate **5** may differ in deionized water and aqueous NaOH. The acidic character of the OH group in fluorinated alcohols is well known; for example, the pK_a of 1,1,1-trifluoroethanol is 12.8 [16]. Intermediate **5** was thus dissociated into $CF_3C(OH)(O^-)C(O)F$ **6** in aqueous NaOH but undissociated in deionized water. Unless dissociated into **6**, $CF_3C(OH)_2C(O)F$ **5** would be further hydrated to $CF_3C(OH)_2C(OH)_2F$ **9**, followed by formation of $CF_3C(OH)_2C(O)O^-$ **11**. In contrast, in aqueous NaOH, most of $CF_3C(OH)_2C(O)F$ **5** was dissociated to $CF_3C(OH)(O^-)C(O)F$ **6**, followed by formation of $CF_3C(O)O^-$ **7** and CO **8**. The intermediate **5** was entirely hydrated to **9** in deionized water, whereas dissociation of **5** to **6** probably hindered hydration of **5** to **9** in aqueous NaOH. Scheme 1 can thus account for the experimental result that hydrolytic degradation products of HFPO differed substantially in deionized water and aqueous NaOH, despite the similarity of the rates of hydrolysis. Scheme 1 can also explain why the yield of carbon monoxide was almost constant (ca. 0.87), independent of the concentration of NaOH in aqueous NaOH. High yields of **7** and **8** in aqueous NaOH (ca. 0.9) suggest that the branching ratio for hydration of **3** to **5** (β; $0 \le \beta \le 1$) was high: $\beta >$ ca. 0.9.

The observed degradation products nearly satisfied material balances for carbon and fluorine (Section 2.4); however, a small amount of mass was missing (less than ca. 10% of the mass). A reason for this missing mass may be formation of $CF_3CF_2C(O)O^-$ **14** through hydrolysis of $CF_3CF_2C(O)F$ **13**, during which an intermediate **12** underwent an intramolecular rearrangement. This hypothetical scheme is based on analogy with the formation of $CCl_3C(O)O^-$ in the hydrolysis of trichloroethylene oxide [10,11].

3.2. Dependence of the rate constants for hydrolysis of HFPO on the assumed values of K_H

The values of the determined parameters (Tables 1 and 2) may depend on the assumed value of K_H. This dependence can be estimated as follows. Under the experimental conditions, the partial pressure of HFPO obeyed Eq. (3). Eq. (3) can also be written as:

$$dP_t / dt = -k_1 P_t \quad (3')$$

Combining this Eq. (3′) with Eqs. (5) and (7) gives Eq. (15).

$$K_H' = C_t / P_t = K_H - k_1 / (a_1 k_m) = K_H - 10^{-3} V_G k_1 / (R T_a k_m) \quad (15)$$

Fig. S2 shows the time series of K_H' values for each experimental run, where the values of C_t and P_t obtained by the fitting procedure were used to calculate the values of K_H'. The values of K_H' were constant, except during the initial period (ca. a few tens of seconds) in each run. This result implies that a quasi-equilibrium state was established for mass transfer of HFPO between the gas and liquid. In that case, Eq. (16) applies because of the requirement for material balance of HFPO.

$$-10^{-3} V_G (R T_a)^{-1} dP_t / dt = k_r K_H' P_t V_L \quad (16)$$

Substituting Eqs. (3′) and (15) into Eq. (16) gives Eq. (17).

$$10^{-3} k_1 V_G/(R T_a) = k_r V_L \times (K_H - 10^3 k_1 V_G/(R T_a k_m)) \quad (17)$$

Rearranging Eq. (17) yields Eq. (18).

$$1 / k_1 = 10^{-3} V_G / (K_H R T_a) \times (1/V_L \times (k_{water} + k_b [OH^-])^{-1} + k_m^{-1}) = 10^{-3} V_G/(R T_a V_L) \times (K_H k_{water} + K_H k_b [OH^-])^{-1} + 10^{-3} V_G/(R T_a) \times (K_H k_m)^{-1} \quad (18)$$

This equation implies that the fitting procedure yielded the products $K_H k_{water}$, $K_H k_b$, and $K_H k_m$ —not values of k_{water}, k_b, and k_m individually— from the time series of partial pressures of HFPO at different concentrations of OH^- and stirring speeds. Accordingly, the values of k_{water} determined by the fitting procedure were inversely proportional to the assumed value of K_H, whereas the product $k_{water} \times K_H$ obtained by the fitting was independent of the assumed values of K_H and would depend only on temperature. Likewise, the determined values of k_b were inversely proportional to the assumed value of K_H, but the product of $k_b \times K_H$ was constant, as was the product of each value of k_m and K_H. Eq. (19) thus gave the value of the product $k_{water} \times K_H$ (s^{-1} M Pa^{-1}) from Eqs. (10) and (11), regardless of the assumed value of K_H.

$$k_{water}(T)\ K_H(T) = 3.7 \times 10^{-11} \times \exp[-3300 \times (T^{-1} - 1/298.2)] \quad (19)$$

3.3. Estimate of tropospheric lifetime of HFPO with respect to hydrolysis in clouds and uptake by the ocean

HFPO was assumed to be a well-mixed species in the troposphere because almost no atmospheric sink has been reported in a peer-reviewed journal. Based on that assumption, the tropospheric lifetime of HFPO with respect to hydrolysis in clouds, τ_{cloud}, and that with respect to uptake by the ocean, τ_{ocean}, were roughly estimated.

First, τ_{cloud} was estimated as follows. The assumed values of K_H and the values of k_{hyd} determined here suggest that hydrolysis in cloud droplets proceeds to the equilibrium predicted by the Henry's law, that is, without mass-transport limitation [17]. Accordingly, removal rates of gaseous HFPO with respect to hydrolysis in cloud droplets, R_{cloud}, were described by Eqs. (20) and (21).

$$R_{cloud} = k_{hyd\text{-}a}\ P_{HFPO} \quad (20)$$

$$k_{hyd\text{-}a} = k_{hyd} \times 10^3\ K_H\ RT\ (\nu_L/\nu_G) / (1 + 10^3\ K_H\ RT\ (\nu_L/\nu_G)) \quad (21)$$

where P_{HFPO} is the partial pressure of HFPO in the atmosphere; R is the universal gas constant; 10^3 is a conversion factor ($dm^3\ m^{-3}$); and ν_L and ν_G are the liquid volume and gas volume, respectively, in clouds. The ratio ν_L/ν_G is the liquid water content of clouds expressed as a dimensionless volume fraction and is typically 3×10^{-7} to 1×10^{-6} [17]. Because $10^3\ K_H RT\nu_L\ /\nu_G \ll 1$ due to the low solubility of HFPO in water, Eq. (21) is approximated by Eq. (22):

$$k_{hyd\text{-}a} = k_{hyd} \times 10^3\ K_H\ RT\ (\nu_L/\nu_G) \quad (22)$$

The value of τ_{cloud} is roughly estimated as follows:

$$\tau_{cloud} = k_{hyd\text{-}a}{}^{-1} / f, \quad (23)$$

where f is the fraction of time that air spends within liquid water clouds in the lower half of the troposphere [18]. From Eq. (19), the product $k_{water} \times K_H$ was calculated to be (1.2–1.8) $\times 10^{-11}\ s^{-1}\ M\ Pa^{-1}$ in the temperature range 270–280 K. By assuming a ν_L/ν_G ratio of 3×10^{-7} and f of 0.15 [18], τ_{cloud} was estimated to be ~17,000–26,000 years. Removal via hydrolysis in clouds is therefore not expected to be a substantial sink of HFPO.

Second, uptake of HFPO by the ocean was evaluated with the use of a two-layer diffusion model on the assumption that diffusive transport occurred in a serial manner across two layers of the surface water, a surface layer with a thickness of ~40 μm above an ~80 m-thick, wave-mixed, turbulent layer characterized by an eddy diffusion coefficient D_O [19]. The lifetime of HFPO in the ocean, τ_{ocean}, was roughly estimated as follows [20,21]:

$$\tau_{ocean} = (r_s + (D_O\ k_{hyd})^{-1/2}) \times H_A / (10^3\ K_H\ R\ T\ f_E) + \tau_{mix} \quad (24)$$

where H_A is the scale height of the troposphere (8000 m); 10^3 is a conversion factor ($dm^3\ m^{-3}$); f_E is the fractional oceanic coverage of the earth's surface (0.7); r_s is the thin film surface resistance to gas uptake at the ocean surface; and τ_{mix} represents the effective mixing time within the troposphere (~45 days). The first term in parenthesis in Eq. (24) is related to the thin-film resistance to mass transport across the air-sea interface, and the second term (in parentheses) is related to the loss of HFPO by hydrolysis during downward diffusion in the ocean mixed layer. Values of r_s depend on turbulence at the air-sea interface which is generated by some factors such as winds over the ocean [22]. Values of r_s vary over time and space. Values of r_s and D_O were assumed to be $1.7 \times 10^4\ s\ m^{-1}$ and $4 \times 10^{-3}\ m^2\ s^{-1}$, respectively [19].

Use of Eq. (24) assumes that hydrolysis decreases the concentration of a species to zero during downward transport of the species in the ocean mixed layer [19,21]. In other words, a necessary condition for the semi-infinite approximation used to derive Eq. (24) is that the eddy-hydrolysis scale depth (H_e) was less than the ocean mixed layer depth, where H_e was defined as follows:

$$H_e = (D_O / k_{hyd})^{1/2} \quad (25)$$

With K_H assigned the reported values of (1.2–1.7) $\times 10^{-8}\ M\ Pa^{-1}$ in the temperature range 280–290 K (Eq. (10)) [15], the values of k_{water} were calculated from Eq. (19) to be (1.1–2.3) $\times 10^{-3}\ s^{-1}$. The lifetime of HFPO in water was then estimated to be 430–910 s in the temperature range 280–290 K. Virtually all the HFPO dissolved in the ocean was therefore assumed to be hydrolyzed in the ocean mixed layer: the calculated values of H_e (1.3–1.9 m) were much less than the assumed ocean mixed layer depth (80 m). Eq. (24) was therefore applicable to HFPO. With K_H assigned the value calculated with Eq. (10) [15], the second term in parenthesis in Eq. (24), $(D_O\ k_{hyd})^{-1/2}$, was calculated with Eq. (19) to be (3.3–4.8) $\times 10^2\ s\ m^{-1}$. In this calculation, k_{hyd} was assumed to be k_{water} because $k_b\ [OH^-]$ is negligible compared to k_{water} in the pH range of seawater. This calculation shows that the value of $(D_O\ k_{hyd})^{-1/2}$ for HFPO is an order of magnitude smaller than the first term in parentheses in Eq. (24), r_s. Values of τ_{ocean} for HFPO are therefore insensitive to k_{hyd} and depend primarily on the values of r_s and K_H. The thin film resistance for mass transport across the air-sea interface is therefore the primary control on the uptake of HFPO by the ocean.

It was beyond the scope of the present study to determine values of r_s and K_H, but by assuming that the solubility of HFPO in seawater was about 80% of its solubility in freshwater because of salting-out effects and that the temperature of the ocean was 286 K, τ_{ocean} was calculated to be ~300 years from Eq. (24) with a K_H of $1.3 \times 10^{-8}\ M\ Pa^{-1}$ and r_s of $1.7 \times 10^4\ s\ m^{-1}$ based on values reported in the literature [15,19]. This estimate may be substantially in error because of the assumption of single values for r_s and solubility; r_s is sensitive to local conditions such as wind speed, and solubility is sensitive to temperature. Nevertheless, this calculation suggests that the hydrolysis of HFPO occurs not in clouds but in the ocean if no processes other than hydrolysis remove HFPO from the atmosphere. The degradation products of HFPO in the ocean are expected to be $CF_3C(OH)_2COOH$ and F^- in the pH range of seawater (ca. 8) as shown in Fig. 10 (Section 2.4). Environmental fate of $CF_3C(OH)_2COOH$ is an issue necessary for future investigation.

4. Conclusions

In deionized water, HFPO was hydrolyzed via Eq. (1) and transformed into $CF_3C(OH)_2COOH$ and F^-. In contrast, in 10–50 mM aqueous NaOH solutions, HFPO was hydrolyzed mainly through Eq. (14): cleavage of the C—C bond occurred, and HFPO was transformed into $CF_3C(O)O^-$ and CO along with F^-. As shown in Scheme 1, the fact that an intermediate $CF_3C(OH)_2C(O)F$ **5** could be dissociated to $CF_3C(OH)(O^-)C(O)F$ **6** only in aqueous NaOH test solutions may explain the distinctly different degradation products in deionized water and aqueous NaOH.

Hydrolysis rates of HFPO increased with increasing concentrations of NaOH in aqueous NaOH, but they were almost independent of the H_2SO_4 concentration in aqueous H_2SO_4 in the H_2SO_4 concentration range 10–30 mM. Based on reported values of K_H (Eq. (10)), the first-order rate constant for the pH-independent hydrolysis of HFPO (k_{water}) at 298.2 K was determined to be (4.2 ± 0.4) $\times 10^{-3}\ s^{-1}$, and the activation energy for this hydrolysis was estimated to be 52 ± 7 kJ mol^{-1}; the bimolecular rate constant for the hydroxide-catalyzed hydrolysis (aqueous reaction with OH^-) of HFPO (k_b) at 298.2 K was determined to be (1.9 ± 0.5) $\times 10^{-1}\ M^{-1}\ s^{-1}$. Eq. (19) gave the temperature-dependent values of the product $K_H \times k_{water}$, regardless of the assumed values of K_H.

On the basis of Eq. (19), the tropospheric lifetime of HFPO with respect to hydrolysis in clouds was estimated to exceed 17,000 years;

therefore, removal via hydrolysis in clouds is probably not a substantial sink of HFPO. The tropospheric lifetime of HFPO with respect to uptake by the ocean was estimated to be some hundreds of years, although this estimate may contain a substantial error. Hydrolysis of HFPO should therefore proceed not in clouds but in the ocean if no processes other than hydrolysis remove HFPO from the atmosphere. The degradation products of HFPO in the ocean are expected to be $CF_3C(OH)_2COOH$ and F^-. Environmental fate of $CF_3C(OH)_2COOH$ is an issue necessary for future investigation.

5. Experimental

5.1. Reagents

HFPO (purity, 97%) supplied from Daikin Industries (Osaka, Japan) was used without further purification. This reagent contained hexafluoropropene as an almost unique impurity; the hexafluoropropene content was determined to be 3.7% from the absorption intensity of a band at 1797 cm^{-1} in the infrared spectrum of this reagent. The absorption coefficient used for this determination was calculated from the reported absorption constants of HFPO integrated between 970 and 1850 cm^{-1} [23]. Carbon monoxide gas (207.3 ppmv in synthetic air) was purchased from Takachiho Chemical Industrial Co. (Tokyo, Japan). Standard aqueous solutions of NaOH (1 M) and H_2SO_4 (1 M) were purchased from Wako Pure Chemical Industries (Osaka, Japan). Water was purified with an EMD Millipore (Billerica, MA, USA) Milli-Q Gradient A10 system (> 18 MΩ cm).

5.2. Closed-circulation reactor experiment

A closed-circulation reactor was used to monitor the decrease of the partial pressure of HFPO with time while an HFPO-air mixture flowed over the test solution. Fig. S3 shows a schematic of the closed-circulation reactor. The reactor has been described in detail before [24], except for its cylindrical glass liquid cell (component d in Fig. S3a), and is described only briefly here.

A test solution such as deionized water (volume, 0.180 dm^3) was introduced into the cylindrical glass liquid cell. The cylindrical glass liquid cell was composed of three parts: a bottom part (86 mm inner diameter and 40 mm high), a middle part (inner diameter gradually decreasing from 86 to 16 mm as the height increased from 40 to 60 mm), and a top part consisting of a tube (16-mm inner diameter and 100-mm length). The bottom part had four baffles (ca. 5-mm length and ca. 10-mm height) at cylindrically symmetric positions on the inner wall. The test solution was typically stirred at 1000 revolutions per minute (rpm) using a polytetrafluoroethylene (PTFE)-coated stirring bar (8-mm diameter × 40-mm length) and a magnetic stirrer. The cylindrical glass liquid cell was placed in a temperature-controlled water bath typically at 295.9 K and was connected to the closed-circulation main system with an Allihn condenser between them. The Allihn condenser was cooled to 275.2 K to suppress diffusion of water vapor from the cylindrical glass liquid cell to the main system.

The HFPO gas mixture was prepared in a two-step procedure by using an absolute pressure meter to dilute HFPO with synthetic air. The initial partial pressure of the HFPO was typically set to ~20 Pa (2×10^{-4} atm), whereas the total pressure of the gas mixture was 1 atm. A magnetically driven glass pump was used to circulate the gas mixture through the reactor at a flow rate of 0.7 dm^3 min^{-1}.

The experimental procedure was as follows. The HFPO gas mixture was circulated for 1 h without contacting the test solution (Fig. S3a; volume, 0.681 dm^3); after 1 h, the gas circulation path was changed so that the gas mixture flowed over the test solution for approximately 9 h (Fig. S3b; volume except for the test solution, 0.962 dm^3). The gas mixture was analyzed every 10 min with a Fourier Transform Infrared (FTIR) spectrometer JEOL Winspec 50 (JEOL Co., Tokyo, Japan) using a White-type multi-reflection cell with an optical path length of 3 m; the spectral resolution was 0.5 cm^{-1} with an acquisition of 64 scans.

At the end of the above period, the reaction products in the test solution were analyzed with an ion chromatograph (Dionex ICS-2100, Thermo Fisher Scientific K.K., Tokyo, Japan) in which an aqueous KOH solution was used at a flow rate of 1.0 mL min^{-1} to elute F^- and other ions from the IonPac AS-20 column (4 mm i.d., 250 mm long) at 308 K. Concentration of KOH in the eluent was gradually increased from 2.5 to 45 mM according to a time program (Fig. S4). If necessary, the aqueous NaOH and aqueous H_2SO_4 test solutions were neutralized with aqueous H_2SO_4 and aqueous NaOH, respectively, for the ion-chromatographic analysis. Ion exclusion chromatography analysis for determination of trifluoroacetate ($CF_3C(O)O^-$) was also performed with an ion chromatograph (Model 8020, Tosoh Co., Tokyo, Japan) in which terephthalic acid (10 mM) was used at a flow rate of 0.6 mL min^{-1} to elute $CF_3C(O)O^-$ from a TSK-gel OApak-A column (7.8 mm i.d., 300 mm long) at 313 K [25].

The partial pressure of HFPO was determined for the observed IR spectrum from the height of the peak at 1162.2 cm^{-1}. Because this peak overlapped part of a peak of hexafluoropropene, the absorbance due to hexafluoropropene was subtracted before determining the partial pressure of HFPO. In making this subtraction, no reaction of hexafluoropropene was presumed to occur. The subtraction reduced the peak height at 1162.2 cm^{-1} by less than 3% in all the IR spectra measured. A calibration curve of HFPO in the partial pressure range examined was prepared using gas mixtures with known partial pressures of HFPO in air. The partial pressure of HFPO, P_{HFPO}, was described by Eq. (26).

$$P_{HFPO} = 23.40 \times h - 3.507 \times h^2, \quad (26)$$

where the units of P_{HFPO} are pascals (Pa), and h is the absorbance (common logarithm) at 1162.2 cm^{-1} for a 3-m path length. The procedure for preparing the calibration curve of HFPO (Fig. S5) is described in the *Supporting Information*.

The partial pressure of carbon monoxide was determined from a calibration curve prepared using standard gas mixtures of carbon monoxide in air. The absorption bands of carbon monoxide overlapped other weak but complex bands that originated from the absorption bands of HFPO and hexafluoropropene in the wavenumber range 2000–2500 cm^{-1}. A loading factor analysis [26] was then used to determine partial pressures of carbon monoxide. Partial pressures of carbon monoxide, P_{CO}, were described by Eq. (27).

$$P_{CO} = 5.405 \times S_{CO} - 0.4877 \times S_{CO}^2 + 0.4311 \times S_{CO}^3, \quad (27)$$

where the units of P_{CO} are pascals and S_{CO} is the score of the loading factor corresponding to the IR spectrum of carbon monoxide at a partial pressure of 5.44 Pa (Fig. S6). Fig. S7 shows the calibration curve of carbon monoxide.

Declarations of interest

None.

Funding

This research did not receive any specific grant from funding agencies in the public, commercial, or not-for-profit sectors.

Acknowledgement

The author thanks Shingo Nakamura (Daikin Industries, Ltd.) for supplying a sample of HFPO.

Appendix A. Supplementary data

Supplementary data associated with this article can be found, in the online version, at https://doi.org/10.1016/j.jfluchem.2018.04.013.

References

[1] H. Millauer, W. Schwertfeger, G. Siegemund, Hexafluoropropene oxide—a key compound in organofluorine chemistry, Angew. Chem. Inter. Ed. Engl. 24 (1985) 161–179.
[2] D. Sianesi, A. Pasetti, F. Tarli, The chemistry of hexafluoropropene epoxide, J. Org. Chem. 31 (1966) 2312–2316.
[3] D.L. Whalen, Mechanisms of hydrolysis and rearrangements of epoxides, Adv. Phys. Org. Chem. 40 (2005) 247–298.
[4] W. Mabey, T. Mill, Critical review of hydrolysis of organic compounds in water under environmental conditions, J. Phys. Chem. Ref. Data 7 (1978) 383–415.
[5] J.N. Brönsted, M. Kilpatrick, M. Kilpatrick, Kinetics studies of ethylene oxides, J. Am. Chem. Soc. 51 (1929) 428–461.
[6] F.A. Long, J.G. Pritchard, Hydrolysis of substituted ethylene oxides in H_2O^{18} solutions, J. Am. Chem. Soc. 78 (1956) 2663–2667.
[7] J.G. Pritchard, F.A. Long, Kinetics and mechanism of the acid-catalyzed hydrolysis of substituted ethylene oxides, J. Am. Chem. Soc. 78 (1956) 2667–2670.
[8] R.A. Conway, G.T. Waggy, M.H. Spiegel, R.L. Berglund, Environmental fate and effects of ethylene oxide, Environ. Sci. Technol. 17 (1983) 107–112.
[9] G.P. Ford, C.T. Smith, Gas-phase hydrolysis of protonated oxirane. Ab initio and semiempirical molecular orbital calculations, J. Am. Chem. Soc. 109 (1987) 1325–1331.
[10] H. Cai, F.P. Guengerich, Mechanism of aqueous decomposition of trichloroethylene oxide, J. Am. Chem. Soc. 121 (1999) 11656–11663.
[11] J. Huang, C.S. Yeung, J. Ma, E.R. Gayner, D.L. Phillips, A computational chemistry investigation of the mechanism of the water-assisted decomposition of trichloroethylene oxide, J. Phys. Chem. A 118 (2014) 1557–1567.
[12] T. Yoshioka, J.A. Krauser, F.P. Guengerich, Tetrachloroethylene oxide: hydrolytic products and reactions with phosphate and lysine, Chem. Res. Toxicol. 15 (2002) 1096–1105.
[13] B. Nozière, M. Kalberer, M. Claeys, J. Allan, B. D'Anna, S. Decesari, E. Finessi, M. Glasius, I. Grgić, J.F. Hamilton, T. Hoffmann, Y. Iinuma, M. Jaoui, A. Kahnt, C.J. Kampf, I. Kourtchev, W. Maenhaut, N. Marsden, S. Saarikoski, J. Schnelle-Kreis, J.D. Surratt, S. Szidat, R. Szmigielski, A. Wisthaler, The molecular identification of organic compounds in the atmosphere: state of the art and challenges, Chem. Rev. 115 (2015) 3919–3983.
[14] O. Levenspiel, Chemical Reaction Engineering, third ed., John Wiley & Sons, NJ, USA, 1999.
[15] R. Sander, Compilation of Henty's law constants (version 4.0) for water as solvent, Atmos. Chem. Phys. 15 (2015) 4399–4981.
[16] R.D. Chambers, Fluorine in Organic Chemistry, John Wiley & Sons, NJ, USA, 2004.
[17] S.E. Schwartz, Mass-transport considerations pertinent to aqueous-phase reactions of gases in liquid-water clouds, in: W. Jaeschke (Ed.), Chemistry of Multiphase Atmospheric Systems, Springer-Verlag, Berlin, 1986, pp. 415–471.
[18] J. Lelieveld, P.J. Crutzen, Influences of cloud photochemical processes on tropospheric ozone, Nature 343 (1990) 227–233.
[19] J.E. Johnson, The lifetime of carbonyl sulfide in the troposphere, Geophys. Res. Let. 8 (1981) 938–940.
[20] W.J. De Bruyn, J.A. Shorter, P. Davidovits, D.R. Worsnop, M.S. Zahniser, C.E. Kolb, Uptake of haloacetyl and carbonyl halides by water surfaces, Environ. Sci. Technol. 29 (1995) 1179–1185.
[21] P.H. Wine, W.L. Chameides, Possible atmospheric lifetimes and chemical reaction mechanisms for selected HCFCs, HFCs, CH_3CCl_3, and their degradation products against dissolution and/or degradation in seawater and cloudwater World Meteorological Organization, Global Ozone Research and Monitoring Project, Report 20, Scientific Assessments of Stratospheric Ozone: 1989 (1990) 272–295.
[22] R. Wanninkhof, Relationship between wind speed and gas exchange over the ocean, J. Geophys. Res. 97 (1992) 7373–7382.
[23] G. Acerboni, J.A. Beukes, N.R. Jensen, J. Hjorth, G. Myhre, C.J. Nielsen, J.K. Sundet, Atmospheric degradation and global warming potentials of three perfluoroalkenes, Atmos. Environ. 35 (2001) 4113–4123.
[24] S. Aoki, S. Kutsuna, K. Murano, Evaluation of the alkaline hydrolysis of HCFC-22 ($CHClF_2$) in a closed-circulation reactor, J. Fluor. Chem. 182 (2016) 127–133.
[25] T. Abe, H. Baba, I. Soloshonok, K. Tanaka, Novel way of separating polyfluorocarboxylic acids by ion-exclusion chromatography, J. Chromatogr. A 884 (2000) 93–103.
[26] E.D. Malinowski, Factor Analysis in Chemistry, third ed., John Wiley & Sons, NJ, USA, 2002.